Nano Research
https://doi.org/10.1007/s12274-018-2011-2
Research Article
ISSN 1998-0124
CN 11-5974/O4

Imaging resolution of biocatalytic activity using nanoscale scanning electrochemical microscopy

José M. Abad[1], Alvaro Y. Tesio[2] (✉), Emiliano Martínez-Periñán[1], Félix Pariente[1], and Encarnación Lorenzo[1,3] (✉)

[1] *Departamento de Química Analítica y Análisis Instrumental, Universidad Autónoma de Madrid, Cantoblanco, 28049 Madrid, Spain*
[2] *Centro de Investigación y Desarrollo en Materiales Avanzados y Almacenamiento de Energía de Jujuy-CIDMEJu (CONICET-Universidad Nacional de Jujuy), Centro de Desarrollo Tecnológico General Savio, Av. Martijena s/n, 4612-Palpalá, Jujuy, Argentina*
[3] *Instituto Madrileño de Estudios Avanzados en Nanociencia (IMDEA-Nanociencia), Campus UAM, Cantoblanco, 28049 Madrid, Spain*

Received: 12 December 2017
Revised: 23 January 2018
Accepted: 23 January 2018

KEYWORDS
scanning electrochemical microscopy,
gold nanoparticle,
redox enzyme,
nanoelectrode,
lactate oxidase

ABSTRACT

Scanning electrochemical microscopy represents a powerful tool for electro(chemical) characterization of surfaces, but its applicability has been limited in most cases at microscale spatial resolution, and the greatest challenge has been the scaling down to the nanoscale for fabrication and the use of nanometer-sized tips. Here, Pt nanoelectrodes with nanometer electroactive area were fabricated and employed for imaging a distribution of gold nanoparticles (AuNPs) and bioelectrocatalytic activity of a redox-active enzyme immobilized on gold surfaces.

1 Introduction

Since it was formally established by Bard et al. [1], scanning electrochemical microscopy (SECM) has been used for a wide range of applications, most of which at a microscale employ ultramicroelectrodes (UMEs) as electrochemical tips [2–6]. One of these applications has been mapping the activity of immobilized enzymes on applicable surfaces because of the practical importance for optimization of biosensors and biochips [7–17]. Characterization of a distribution of immobilized enzymes has been carried out either in feedback (FB) mode [11–15] or in generation-collection (GC) mode [16–18]. In the FB mode for redox activity mapping, the UME probe is used to oxidize or reduce a reversible electron redox mediator by applying a potential at which diffusion-controlled conversion proceeds at the same time as the tip scans

Address correspondence to Encarnación Lorenzo, encarnacion.lorenzo@uam.es; Alvaro Y. Tesio, atesio@cidmeju.unju.edu.ar

the surface. The FB process occurs when the tip-generated redox mediator diffuses into the sample and is returned to its original oxidation state through the enzymatic reaction catalyzed by an immobilized enzyme. Next, the mediator diffuses back to the tip, thus establishing an FB loop and giving rise to an electrocatalytic current at the UME. This mode of operation has been implemented for oxidoreductase enzymes where electron transfer between the active site of the enzyme and UME is facilitated by the presence of the redox mediator. In GC mode, the UME is applied either to detect the redox-active product generated at the surface of the sample after enzymatic conversion of a substrate or for generating the latter. Thus, it can be employed for investigating any enzyme able to generate or deplete any electroactive substance near the sample surface.

Both SECM modes have enabled imaging of the relative positions of bioactive surfaces modified by enzymes but only on the micron length scale. In recent years, many efforts have been made for improving their spatial resolution by scaling down to the nano-scale where researchers tried to develop a powerful technique in the field of characterization by scanning probe microscopy at that level. Progress has been stimulated by advances in fabrication of geometrically well-defined nanoelectrodes from different materials, with Pt electrodes mostly serving as SECM tips [19–21]. These nanoelectrodes offer great advantages such as enhanced mass transport rates, a decrease in the double-layer capacitance, and an enhanced signal-to-noise ratio [22, 23]. Nonetheless, these electrodes are much harder to produce and to use than micron-sized ones. The methods of fabrication reported are usually based on top–down approaches similar to those employed for UME and consist of sharpening of a micrometer Pt wire by either electrochemical etching [24–28] or by laser pulling [20, 21, 29–33] to obtain a sharp point. Subsequently, it is insulated off except for the end of the tip by coating with an insulating material such as an electrophoretic paint [25, 26,30, 31, 34–36], polyimide [37], Teflon [38], apiezon wax [39–41], or glass [21, 27, 42] or by electropolymerization of a polymer thus scaling down to a nanometer size [43]. Despite these significant fabrication advantages, at present, the use of SECM at the nanoscale for imaging the topography and/or activity of a surface modified with nanomaterials (metal nanoparticles (NPs) or enzymes) at single-particle and/or single-molecule resolution remains a challenge for many applications. So far, only a few research groups have attempted electrochemical detection of stand-alone electroactive molecules in solution [39–41] or stand-alone NPs electrodeposited on a substrate [44]. Unwin et al. have conducted scanning electrochemical cell microscopy to map the reactivity of individual 100 nm metal NPs within an electrocatalytic ensemble by means of an UME [45]. More recently, Bard et al. tested nanometer-scale SECM for the study of geometric properties and catalytic activity of Pt NPs in the hydrogen oxidation reaction [46].

We have previously reported [47] patterned arrays of gold nanoparticles (AuNPs) prepared via SECM by electrochemical reduction of a gold salt at a platinum UME.

Herein, we want to go a step further and report the capacity of SECM for imaging of a distribution of AuNPs and redox-active enzymes attached to gold surfaces at the nanometer scale by means of Pt nano-electrodes. The aim of this work was to show the potential utility of this technique when nanotips serve as imaging probes.

2 Experimental

2.1 Chemicals and materials

Lactate oxidase (LOx; EC 232-841-6, from Pediococcus species) lyophilized powder containing 41 $U \cdot mg^{-1}$ solid matter was bought from Sigma Chemical Co. (St. Louis, MO, USA). A stock solution was prepared by dissolving 1.3 mg of the LOx lyophilized powder in 250 μL of 0.1 M phosphate buffer (pH 7.0), was aliquoted (10 μL), and was stored at –30 ˚C. L-(+)-Lactic acid lithium salt (97%), hydroxymethylferrocene (HMF), potassium hexachloroiridate (IV) technical grade, phenol (99%), 3,3-dithiodipropionic acid di(N-succinimidyl ester) (DTSP), and potassium chloride were purchased from Sigma-Aldrich and were used as received. Sodium phosphate (Merck) was employed for the preparation of buffer solutions (0.1 M, pH 7.0). 1-Hexanethiol (97%) and 1,9-nonanedithiol (99%) were acquired from Alfa

Aesar and Sigma-Aldrich, respectively. Water was purified with a Millipore Milli-Q system. All solutions were prepared immediately prior to use with ultrapure water and passed through a syringe filter with 100 nm pore size (Millex-Syringe driven filter unit, PVDF-0.1 μm, Merck Millipore Ltd.). The SECM cell made of Teflon, the gold substrates, and all the glassware were cleaned by exposure to the "piranha" solution (concentrated H_2SO_4 with a 30% H_2O_2 solution at 3:1) followed by exhaustive rinsing with ultrapure water. (Caution: The piranha solution reacts violently with most organic materials and may result in explosion or skin burns if not handled with extreme caution.)

2.2 Pt nanoelectrode fabrication

Pt nanoelectrodes serving as nanotips in SECM were fabricated using a pipette puller (PE-21, Narishige group). An approximately 20 mm long Pt wire with 25 μm diameter (Alfa Aesar, 99.95%) was inserted into a 100 mm long glass capillary with an outer diameter of 1.2 mm and an inner diameter of 0.68 mm in such a way that the Pt wire was located in the middle part of the capillary. The glass capillary was placed at the center of the heater in the puller chamber. The following values served for adjusting the heater level and the magnet level to produce the preferred electrodes: Heater, 50; Sub-magnet, 10; MainMagnet, 100. Electrical connection to the inside end of the Pt wire to a copper wire was made with silver epoxy.

2.3 Preparation of DTSP-functionalized gold substrates

Gold substrates were immersed for 3 h in a 1 mM solution of DTSP in dimethyl sulfoxide. The electrodes were subsequently rinsed with dimethyl sulfoxide and acetone and dried in nitrogen.

2.4 Immobilization of LOx on gold substrates

DTSP-functionalized and bare gold substrates were modified with the enzyme by placing 10 μL of the LOx stock solution onto the surface and leaving it there to react for 1 h. The electrode was next washed with 0.1 M phosphate buffer (pH 7.0) and finally with ultrapure water.

2.5 SECM

These measurements were carried out under a CH Instruments model 900B scanning electrochemical microscope placed on an antivibration table. The electrochemical cell was located on a *XYZ* positioning stage and the distance between the tip and the sample was controlled by a stepper motor (coarse approach) combined with a piezoelectric nanopositioning system (fine approach; *X*, *Y*, and *Z* resolution: 1.6 nm; Newport 423 series). All voltammetry and SECM measurements were performed in a grounded Faraday cage using a three-electrode configuration consisting of a Pt wire auxiliary electrode, Ag/AgCl saturated reference electrode, and the fabricated Pt UME.

The sample substrates were made of glass (1.1 cm × 1.1 cm) covered with evaporated gold layers (0.2–0.3 μm) deposited over a chromium adhesion layer (Gold Arrandee™) suitable for flame annealing procedure (2 min in a gas flame), which is used to obtain Au (111) terraces.

2.6 Scanning electron microscopy (SEM)

This imaging was conducted under a field emission scanning electron microscope, FE-SEM FEI Nova NANOSEM 230.

2.7 Atomic force microscopy (AFM)

This procedure was performed on a Nanoscope IIIa apparatus from Digital Instruments (DI, Santa Barbara, CA, USA) with a scanner having a maximal scan range of ~ 14 μm operating in tapping mode in air.

3 Results and discussion

3.1 Nanoelectrode fabrication

Pt nanotips were fabricated by a two-step process starting with heating and simultaneously pulling a 25 μm Pt microwire inserted into a borosilicate glass capillary as described in the Experimental section. As the glass was drawn out, the metal thinned, thereby drastically reducing the radius of the wire and providing a close-fitting seal between the glass and the metal wire inside it (Fig. 1(a)). By this method, each

capillary–microwire section produces two needle-shaped electrodes. The shape and size of the electrodes after the pulling process were examined by optical microscopy and by SEM. Figure 1(b) shows an SEM image of a typical Pt nanoelectrode obtained by the proposed method. Readers can see that the electrode area has an almost hemispherical shape, and the radius was roughly measured and found to be ~ 120 nm.

To reduce the exposed metal surface to obtain electrodes having electroactive areas in the nanoscale range, a subsequent step of insulation by electrochemical polymerization of phenol was performed [48]. Electropolymerization was carried out by dipping the Pt tip in a solution containing 0.1 mM phenol in 0.5 M H_2SO_4 and by scanning in the potential range from 0.7 to 1.3 V by cyclic voltammetry at low scan rates (5 mV·s^{-1}). Figure 1(c) shows the obtained cyclic voltammograms, where the observed anodic peak at 1.2 V corresponds to the irreversible phenol electrooxidation. After the first scan, a noticeable decrease in the current was observed owing to the formation of a nonconductive polymeric film leading to passivation of most of the electrode surface. The electropolymerization of phenol via its oxidation to quinones is a complex process involving formation of phenoxy radicals as intermediates on the Pt surface. These films have been reported to be chemically inert, hard, and thermally stable [48].

After that, the electrodes were characterized by their voltammetric responses corresponding to the reduction of 1 mM K_2IrCl_6 in 0.1 M KCl. Both electrode responses after the pulling process (Fig. 2(a)) and after electropolymerization (Fig. 2(b)) showed well-shaped sigmoidal curves and a small charging current. No response was observed in a 0.1 M KCl electrolyte solution. The radius of the electrochemical active surface of the nanoelectrodes was calculated from the steady-state limiting current, i_{lim}, assuming a hemispherical geometry via the following equation

$$i_{lim} = 2\pi nFDC^*r_{app} \quad (1)$$

where C^* and D are the bulk concentration (1 mM) and diffusion coefficient ([8.2 ± 0.4] × 10^{-6} cm^2·s^{-1}) [49] of $IrCl_6^{2-}$, respectively; r_{app} is the apparent radius of the exposed section of the tip; n is the number of electrons transferred per molecule (in this case one electron); and F is Faraday's constant. The apparent or effective electrochemical radius of the electrode is

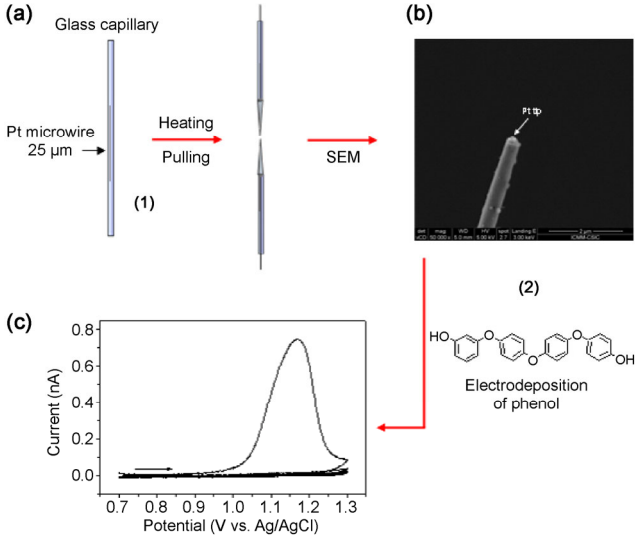

Figure 1 (a) A general scheme showing the two steps of fabrication of the nanoelectrodes: (1) pulling of a 25 μm Pt microwire inserted in a glass capillary, (2) insulation of the Pt tip by electropolymerization of phenol. (b) A SEM image of the Pt electrode (radius, ~ 120 nm). (c) Cyclic voltammograms of the Pt tip in a solution containing 0.1 mM phenol in 0.5 M H_2SO_4 at a scan rate of 5 mV·s^{-1}.

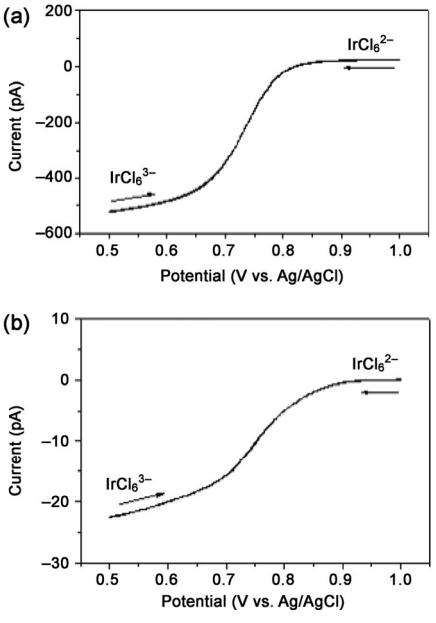

Figure 2 Electrochemical characterization of Pt nanoelectrodes by cyclic voltammetry in 1 mM hexachloroiridate (IV) and 0.1 M KCl at a scan rate of 10 mV·s^{-1} (a) before (radius, ~ 110 nm) and (b) after tip insulation by electrodeposition of phenol (resultant radius, ~ 5 nm).

controlled by the number of electropolymerization cycles performed. Typically, five cycles at 5 mV·s^{-1} were enough to drastically reduce the electroactive surface, thereby decreasing the electrode radius from ~ 110 to ~ 5 nm. The results in Fig. 2 indicate that electrodes of nanometer dimensions can be readily fabricated by this procedure.

3.2 AuNP imaging

To evaluate the effective resolution of the nanoelectrodes under the scanning electrochemical microscope, they were applied to detecting AuNPs attached to an insulated gold surface (Scheme 1) according to the matrix isolation method similar to that reported for measuring the conductance of a dithiol molecule embedded in a monothiol self-assembled monolayer (SAM) by scanning tunneling microscopy [50]. The gold surface was flame-annealed beforehand to obtain Au (111) terraces and later modified with an SAM of hexanethiol by immersion in a 20 mM ethanol solution for 48 h for obtaining the insulation of the surface through the chemisorption of thiolate groups. Next, some of these alkanethiol molecules were replaced via a ligand exchange reaction with 1,9-nonanedithiol molecules at different reaction periods (5–20 min) to provide a suitable –SH terminal groups for anchoring $(C_8H_{17})_4N^+Br^-$-stabilized AuNPs of 5 ± 1 nm diameter presynthesized according to a previously described method. [51]. The coverage of the gold surface by the nanoparticles was ascertained by AFM and SEM. We found that both the rate and extent of ligand exchange and therefore the nanoparticle coverage were dependent on duration of the reaction between a hexanethiol SAM-covered gold surface and the dithiol. Figure 3(a) shows an AFM image of a hexanethiol-gold surface immersed for 20 min in a 2 mM dithiol solution and next, after thorough rinsing with ethanol, in a 1 nM toluene solution of AuNPs for 5 min. Readers can see that the surface is completely covered by AuNPs. The line-height profile (inset in Fig. 3(a)) of the image reveals heights of the AuNPs of 5–10 nm and widths (diameter or full width at half-maximum) of 18–24 nm.

This surface was then scanned by SECM followed by electrochemical reduction of 1 mM K_2IrCl_6 in 0.1 M KCl by applying a potential of +0.5 V at the tip while the surface was kept unbiased. At this potential, the hexachloroiridate (IV) ion can be reduced to hexachloroiridate (III). Achieving nanometer resolution is needed to operate at a tip–sample distance of a few nanometers to make sure that the SECM tip is placed properly within the range of the modulation of the hemispherical diffusion profile in front of the electrode. At this distance, only the electroactive area close enough to the gold surface modified with AuNPs with respect to the overall area (estimated from the steady-state voltammetric limiting current) will give a sensitive response for surface imaging. In this manner, the tip was brought to close proximity with the surface first via a coarse approach and then an extremely fine piezoelectric control before the scanning process. Figure 3(b) illustrates the approach curve recorded with high accuracy via a slow approach (20 to 1 nm·s^{-1}) of the tip toward the sample surface after the electrochemical reduction of K_2IrCl_6. When the tip was positioned at a relatively long distance from the surface, $d > 10r_{app}$, a steady-state current, $i(\infty)$, was rapidly established due to hemispherical diffusion of the $IrCl_6^{2-}$ ions.

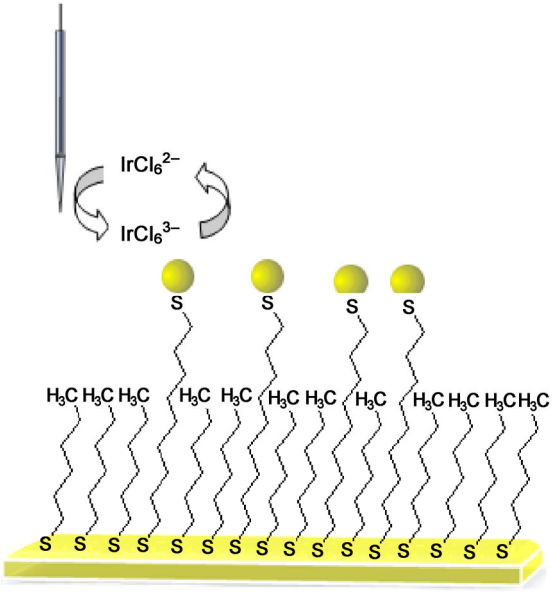

Scheme 1 A schematic drawing of single-nanoparticle detection (by SECM in FB mode in 1 mM K_2IrCl_6) of a gold surface modified with a mixed SAM of hexanethiol and 1,9-nonanedithiol with subsequent attachment of AuNPs of 5 ± 1 nm diameter. The structures are not drawn to scale.

This current remained constant at 26.0 ± 0.2 pA with negligible electrochemical noise until the tip was brought close enough to the surface covered by the hexanethiol SAM where diffusion to the nanoelectrode was hindered and the steady-state current, i, decreased as compared to $i(\infty)$ according to a negative FB process.

Once the distance between tip and substrate, d, approached almost zero, the SECM tip was moved in the X–Y direction (500 nm × 500 nm) while the Z position was maintained constant. This distance was optimized and tracked. A stable tip current was monitored to ensure a stable nanogap between the tip and the sample before SECM imaging. The short distance in the X–Y sweep ensures that the distance along the Z direction remains constant throughout the sweep. The SECM image of the surface (Fig. 3(c)) appears to be full of peaks due to increasing tip currents arising from the surface as a consequence of the positive FB produced by AuNPs when the tip was positioned over them. Redox probe moieties of $IrCl_6^{2-}$ were reduced at the nanoelectrode and oxidized at the nanoparticle surface causing a large current. This effect can be more clearly observed in the topographical

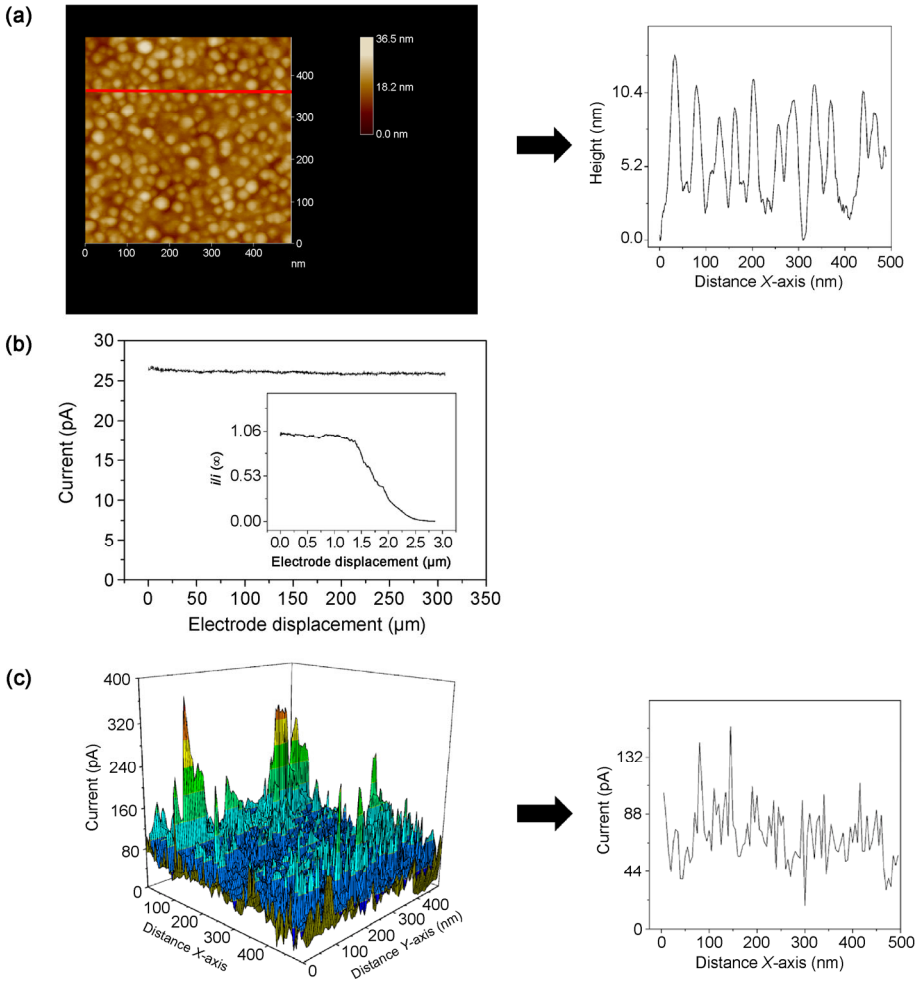

Figure 3 (a) An AFM image of a hexanethiol SAM-covered gold surface after 20 min of a reaction in a 2 mM 1,9-nonanedithiol solution and then in a 1 nM AuNP (5 ± 1 nm) solution for 5 min. The inset shows the topographic surface profile. (b) A coarse approach curve for a hexanethiol-modified gold surface via electrochemical reduction of 1 mM K_2IrCl_6 in 0.1 M KCl, when a potential of +0.5 V was applied at the tip, and the surface was kept unbiased. Inset: a piezoelectric approach curve recorded with high accuracy via a slow approach (at 1 nm·s^{-1}) of the nanoelectrode toward the sample surface. The current was normalized: $i/i(\infty)$. (c) SECM mapping of the AuNP-modified SAM surface obtained in feedback mode in 1 mM K_2IrCl_6 and 0.1 M KCl when a tip potential of 0.5 V was applied. The inset shows the current profile along the X-axis obtained at 300 nm (Y-axis).

surface profile (inset in Fig. 3(c)) obtained along the *X*-axis, which shows peak current responses with a width at half the maximum ranging from approximately 5 to 10 nm, indicating the capacity of the tip for distinguishing the presence of stand-alone or associated nanoparticles immobilized on the surface. In this case, the lateral resolution was higher than that obtained by AFM, thereby allowing us to sense double particles (~ 35 vs. ~ 17) per unit area of the scan. These results suggest that SECM microscopy by scaling down can generate a topographical image of the surface at nanoscale resolution.

Similar experiments were carried out for AuNP-modified gold surfaces, which decreased the reaction time of the thiol exchange. A SEM image (Fig. 4(a)) of a hexanethiol-modified gold surface with subsequent incubation with 2 mM 1,9-nonanedithiol for 15 min and then for 5 min in a 1 nM AuNP solution reveals that in this case, the surface is partially covered by scattered rosary bead-shaped AuNPs. The measured tip current in the SECM scan should be sensitive to this particle coverage of the surface, and hence only a smaller number of AuNPs is expected to be detected. The scan of the surface along the *X*-axis (Fig. 4(b)) shows the electrochemical response obtained in the absence or presence of linked AuNPs. In the absence (Fig. 4(b), black curve), the current remained constant corresponding to insulation behavior showing complete blocking of the surface by the attached mixed-SAM and indicating that this layer is almost defect-free. On the contrary, when the tip was positioned over areas modified with the nanoparticles, an increasing tip current due to the positive FB produced by AuNPs was observed, giving rise to a series of peaks (Fig. 4(b), red curve). It is noticeable that the peaks are detectable only after attachment of AuNPs to the dithiol-modified gold surface, and they are in agreement with the peaks expected on the basis of the nanoparticle distribution observed by SEM.

After the duration of the reaction of hexanethiol exchange with 1,9-nonanedithiol was decreased even more (to 5 min), the SECM mapping of the surface (Fig. 5(a)) modified with AuNPs yielded two remarkable findings. First, it was possible to topographically visualize the surface (at the nanoscale) that was formed by flat terraces and steps. The image obtained corresponds to an inverted version of the real one because a lower current indicates smaller distances between the tip and the insulated sample. Second, an increase in tip currents associated with AuNPs, as shown in the topographic *Y*-axis profile in Fig. 5(b), was obtained only at the boundary between the terrace and the step. This is more clearly illustrated in the *X*-axis profile (Fig. 5(c)) where the peak at 220 nm with a width of 6 nm at half the maximum can be ascribed to the attachment of a single nanoparticle at this step.

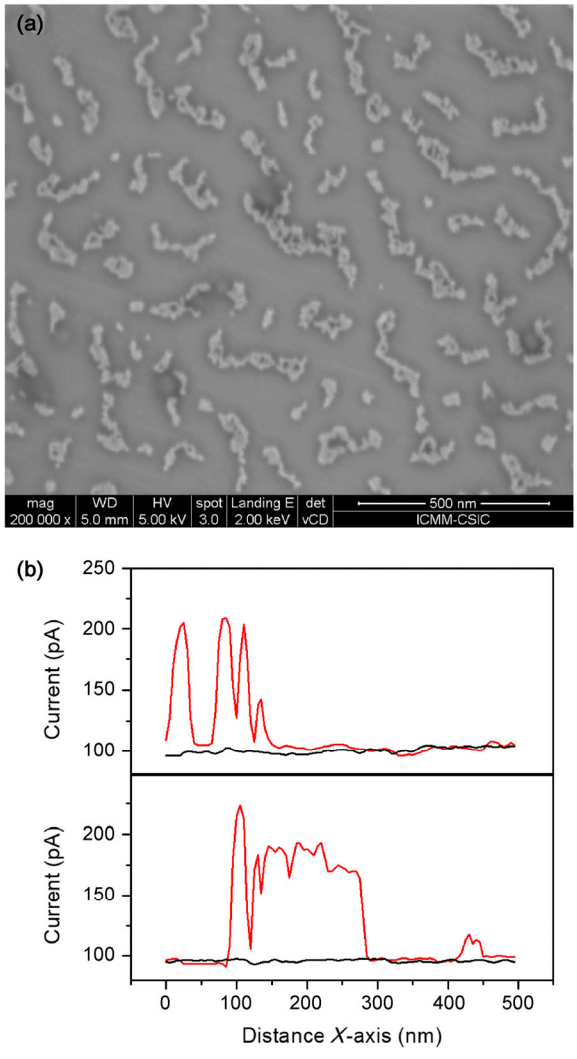

Figure 4 (a) A SEM image of a hexanethiol SAM-covered gold surface after 15 min of a reaction in a 2 mM 1,9-nonanedithiol solution and then in a 1 nM AuNP (5 ± 1 nm) solution for 5 min. (b) SECM *X*-axis scans across of the surface in FB mode in 1 mM K_2IrCl_6 and 0.1 M KCl (red curve) when a tip potential of 0.5 V was applied. Black curves correspond to the area without AuNPs.

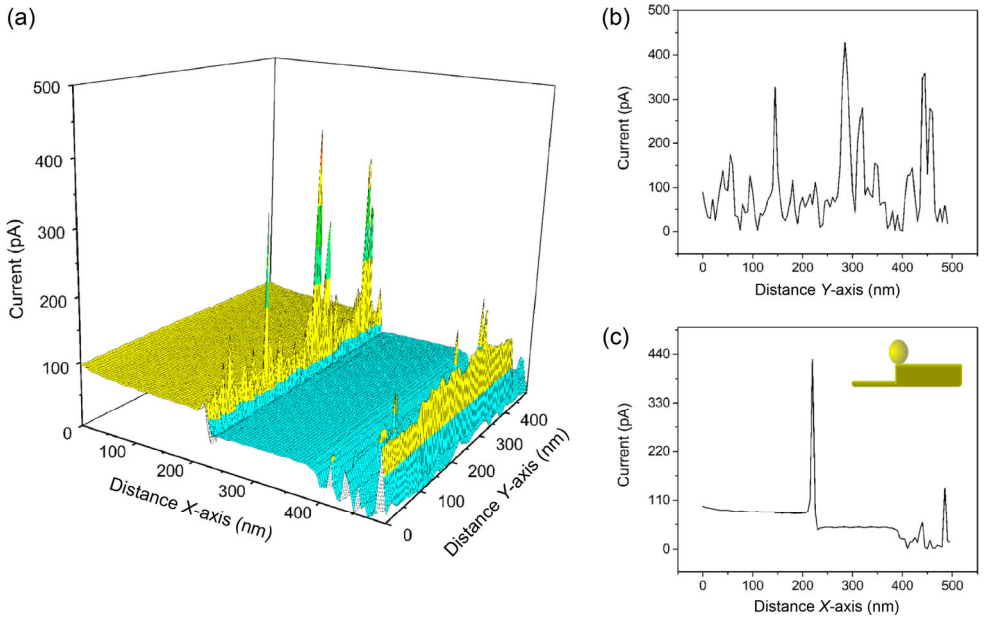

Figure 5 (a) An SECM mapping image in feedback mode in 1 mM K_2IrCl_6 and 0.1 M KCl when a tip potential of 0.5 V was applied to a hexanethiol SAM-covered gold surface after 5 min of a reaction in a 2 mM 1,9-nonanedithiol solution and then in a 1 nM AuNP (5 ± 1 nm) solution for 5 min. Current profiles along (b) the *Y*-axis obtained at 220 nm (*X*-axis) or (c) the *X*-axis obtained at 285 nm (*Y*-axis), corresponding to the AuNPs immobilized on the step and schematic drawing (inset).

These data suggest that the rate of place exchange by dithiol and subsequent AuNP attachment is more rapid for Au sites at vertices and edges of the core surface ("defect" sites) than at core terrace sites being observed at short reaction periods. This result was expected because it has been reported that SAMs formed on metal substrates in regions where the topography changes drastically—edges of topographical features—induce a higher degree of disorder, and thus the thiolates in these regions are easier to exchange with other thiols by displacement [52, 53]. It is noteworthy that the fabricated SECM electrodes have an effective nanometer resolution enabling (at this level) topographical imaging of the surface aside from examination of the cross-sectional profile and any sharp changes in the topography.

3.3 Mapping of LOx activity

A key challenge in bioelectrochemical research for fundamental studies of enzymatic catalysis and biotechnological applications is to control the organization of proteins on electrode surfaces while maintaining their biological activity [54]. SECM seems to represent an excellent tool for evaluating the distribution of an active immobilized enzyme on an electrode surface, in particular if nanometer resolution can be achieved. By means of the as-fabricated Pt nanotips, the concept of imaging the activity of an immobilized enzyme at the nanoscale level by SECM was validated here by analyzing the redox activity of LOx immobilized on a gold surface (Scheme 2). Among the different methods described in this work to achieve the enzyme immobilization, LOx was either physically adsorbed directly onto a gold surface (LOx-Au) or immobilized by covalent bonding on a gold surface prefunctionalized with DTSP (LOx-functionalized-Au). Given that DTSP adsorbs onto gold surfaces through the disulfide group forming a SAM, the terminal succinimidyl groups are exposed to the solution allowing for subsequent covalent immobilization through lysine residues of LOx [55].

Pt tips at nanometer resolution were again first brought into close proximity with the enzyme-modified gold surfaces with high accuracy via oxidation of HMF serving as a redox mediator in solution, by applying a potential of +0.6 V.

As depicted in Scheme 2(a), in the presence of oxygen, the enzyme catalyzes oxidation of lactate to

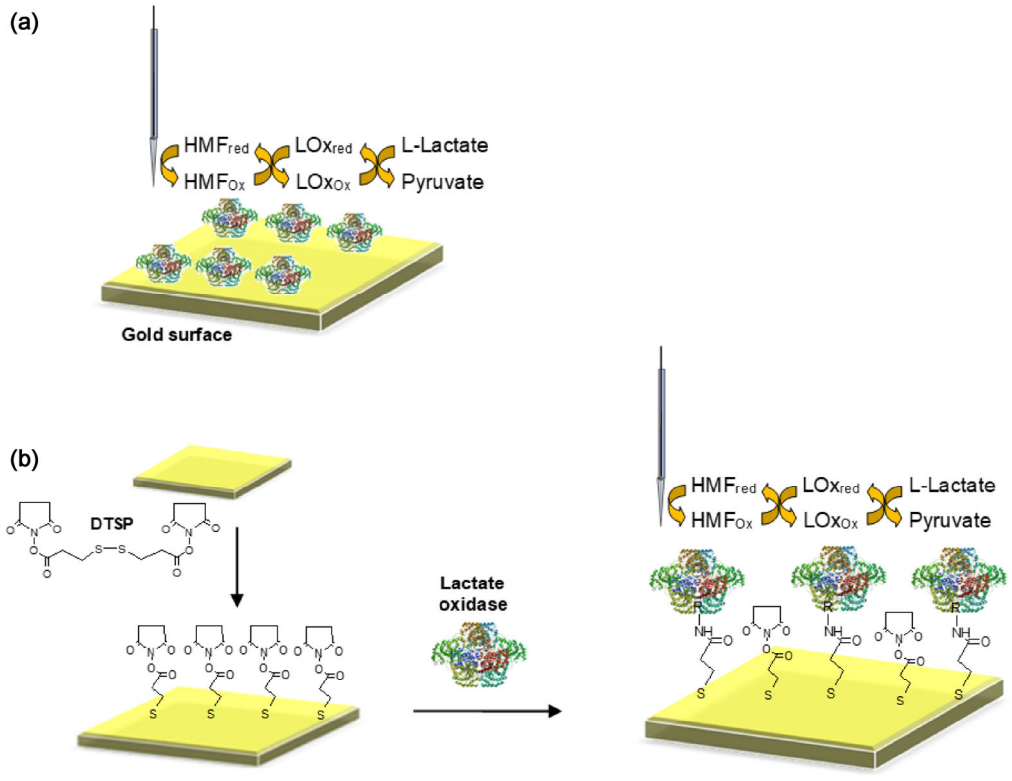

Scheme 2 A schematic drawing of single-redox enzyme detection by SECM: LOx was physically adsorbed directly onto a gold substrate (a) or immobilized by covalent bonding on a gold surface prefunctionalized with DTSP (b). Positive-FB mode was employed with hydroxymethylferrocene as a redox mediator and L-lactate as an enzymatic substrate. The structures are not drawn to scale. LOx structure was obtained from the Protein Data Bank [56].

pyruvate, while the electrons involved in the process are immediately transferred to the oxidized form of the soluble redox mediator (HMF), regenerating the enzymatic activity. The reoxidation of HMF on the electrode surface leads to a biocatalytic current indicative of the biocatalytic activity. The use of redox mediators in solution is a way to detect the enzymatic activity at lower potentials than those required after the reaction is followed by oxidation of the side product H_2O_2.

Figure 6(a) shows the approach curve recorded until the distance between the tip and surface was almost zero. In this case, as the tip was brought close to a conductive surface, and the oxidized form of HMF generated at the tip was reduced at the surface and diffused back to the tip, thus causing a higher current than that obtained when the tip was far away. This distance was optimized beforehand to perform the following experiments. Once the tip was brought into close proximity with the sample at the optimal nanometer distance, SECM responses to the LOx-modified surfaces in positive FB mode, either in the presence or absence of the enzymatic substrate (L-lactic acid), were employed to image the catalytic activity of these enzyme electrodes.

Figures 6(b) and 6(c) show SECM images of a scanned area of 100 nm × 50 nm of a bare gold substrate after adsorption of LOx in the absence (b) or presence (c) of lactate. In the absence of the enzymatic substrate, the only faradic response observed corresponded to the oxidation of HMF by the tip, and this process remained homogeneous over the surface.

By contrast, when the same area was scanned after addition of lactate, a series of clear-cut individual peaks were obtained. They can be ascribed to the electrocatalytic reduction current of the HMF by the LOx upon its reduction by lactate. These are important results because they allow us to image the relative positions of catalytically active LOx molecules on the surface via their enzymatic activity and thus provide

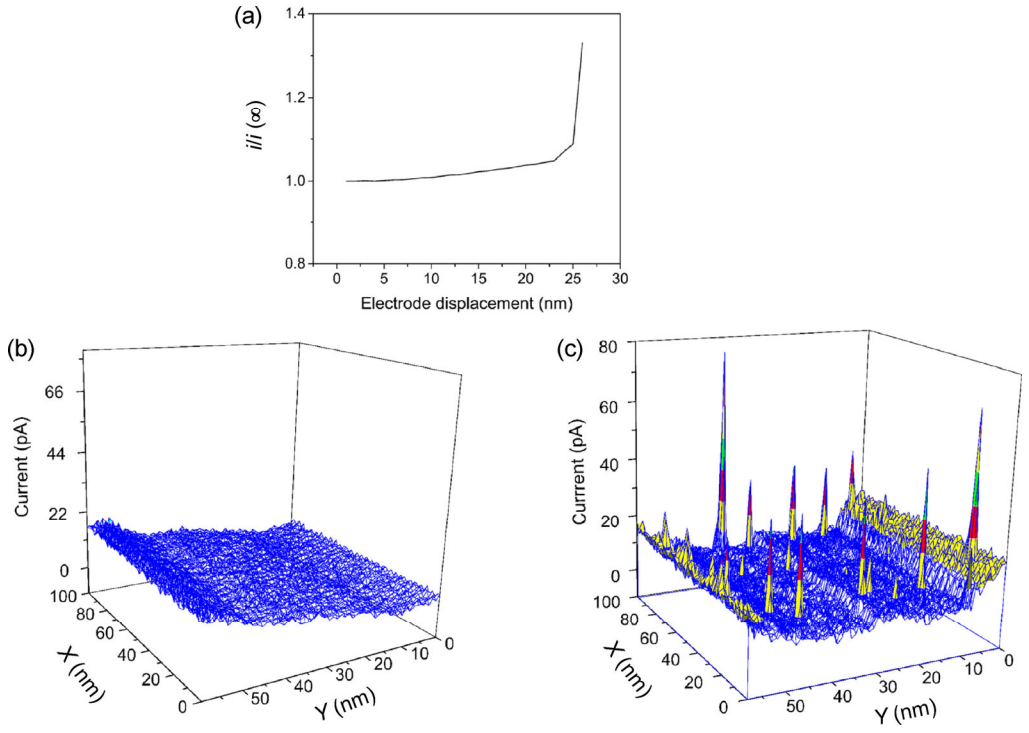

Figure 6 (a) The curve of an approach to an enzyme-modified gold surface via oxidation of 1 mM HMF in 0.1 M phosphate buffer (pH 7.0) containing 0.1 M KCl and when a tip potential of 0.6 V was applied and the surface was kept unbiased. Approach rate: 1 nm·s^{-1}. The current was normalized: $i/i(\infty)$. (b) and (c) SECM mapping images obtained in FB mode of a bare gold surface after direct adsorption of LOx protein before (b) and after addition of L-lactate (c) at a final concentration of 1 mM, by means of 1 mM HMF in 0.1 M phosphate buffer (pH 7.0) containing 0.1 M KCl when a tip potential of 0.6 V was applied.

clear evidence of the amount of the functional adsorbed enzyme. In this case, a small amount of the active enzyme was observed as a consequence of the immobilization process (direct adsorption of LOx). The physical adsorption processes are based on hydrophobic or electrostatic interactions between the proteins and the gold surface in a nonspecific manner and can presumably cause subsequent protein denaturation leading to a loss of most of enzymatic activity.

Similar SECM imaging experiments were conducted with a gold electrode modified with a SAM of DTSP after incubation with LOx. As presented in Fig. 7(a), in the absence of lactate, no electrocatalytical response was observed, and the measured current was again due to the HMF oxidation by the tip. This anodic current was also homogeneous over the *X*–*Y* axis scanned area, thereby showing complete blocking of the surface by the attached SAM. In contrast, the addition of lactate caused appearance of a stripe-like pattern formed by ordered hill–valley structures parallel to the scan direction as a consequence of the electrocatalytic reduction of HMF by the immobilized molecules of the protein (Fig. 7(b)). The width of the stripes was found to be 12 ± 4 nm, which is close to the size reported for the LOx dimensions (the overall dimensions of each tetramer are 50 Å × 100 Å × 100 Å) [56]. The same area was also scanned in the vertical direction (*Y*–*X* scan), and the same types of structures were observed (Fig. 7(c)). These results suggest that the scanned surface is densely covered by the monolayer protein on the ordered DTSP-SAM, where the immobilized LOx molecules are so close to each other (i.e., separated by a minimal distance). In this scenario, the tip is able to distinguish only between either arrows or columns formed by enzyme molecules depending on the scan direction.

It is also noteworthy that the SECM image of the DTSP-Au surface upon covalent immobilization of LOx shows a structure different from that observed with direct adsorption. This finding is in agreement with that observed in AFM experiments reported in a previous work [57], where the tip–protein interaction

assays based on force curves indicated that the protein geometry of adsorption in both systems was different. The covalent immobilization through N-hydroxysuccinimidyl-terminated SAM gives rise to a close-packed arrangement of the active immobilized enzyme thus preventing denaturation.

The latter experiments indicate that with SECM activity mapping at nanoscale resolution, it is possible to determine how effective various protein immobilization methods are in terms of stability and preservation of a protein's vital activities during the immobilization step.

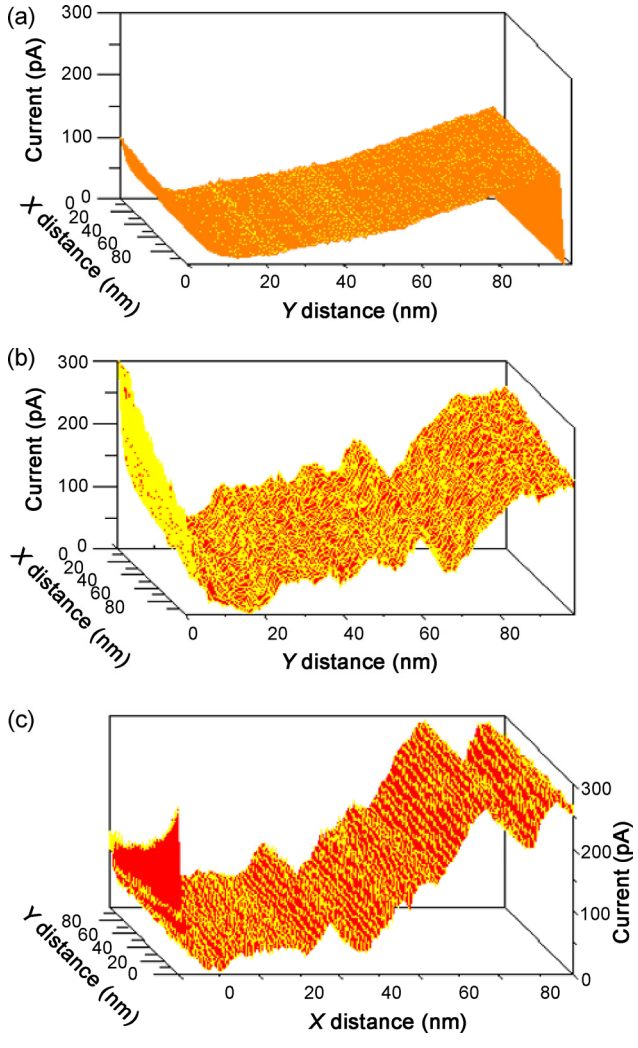

Figure 7 SECM mapping images (obtained in positive FB mode) of a DTSP SAM-covered gold surface after immobilization of LOx protein before (a) and after addition of L-lactate at a final concentration of 1 mM. (b) *X*–*Y* and (c) *Y*–*X* scan direction when 1 mM HMF was tested in 0.1 M phosphate buffer (pH 7.0) containing 0.1 M KCl and a tip potential of 0.6 V was applied.

4 Conclusions

In summary, we successfully fabricated Pt nanotips with effective nanometer resolution, and they enable imaging of both a distribution of conductive nanomaterials such as AuNPs and the biocatalytic activity of LOx immobilized on gold surfaces. Furthermore, they allow for topography characterization of gold surfaces, either bare or modified with SAMs, in terms of reactivity in a thiol exchange reaction, thereby detecting the presence of topographical features on the core surface such as edges or vertices. We expect that this important advance in the use of SECM will make this technique possible at a nanoscale level for a wide range of applications, including studies of electrocatalysis, corrosion, and other biological systems.

Acknowledgements

J. M. A. acknowledges research funding by a "Ramon y Cajal" contract from the Spanish Ministry of Science and Innovation. A. Y. T. acknowledges a fellowship from CONICET and Fundación Carolina. We are grateful to Prof. Luis Vázquez and Tech. Andrés Valera (ICMM-CSIC) for carrying out AFM and SEM measurements, respectively. The authors also thank Dr. Elena Casero (UAM) for support in the use of SECM instrumentation and Prof. H. D. Abruña for critically reviewing this manuscript.

References

[1] Bard, A. J.; Fan, F. R. F.; Kwak, J.; Lev, O. Scanning electrochemical microscopy. Introduction and principles. *Anal. Chem.* **1989**, *61*, 132–138.

[2] *Scanning Electrochemical Microscopy*; Mirkin, M. V.; Bard, A. J., Eds.; Marcel Dekker: New York, 2001.

[3] Wittstock, G.; Burchardt, M.; Pust, S. E.; Shen, Y.; Zhao, C. Scanning electrochemical microscopy for direct imaging of reaction rates. *Angew. Chem., Int. Ed.* **2007**, *46*, 1584–1617.

[4] Takahashi, Y.; Hirano, Y.; Yasukawa, T.; Shiku, H.; Yamada, H.; Matsue, T. Topographic, electrochemical, and optical images captured using standing approach mode scanning electrochemical/optical microscopy. *Langmuir* **2006**, *22*, 10299–10306.

[5] Tan, C.; Rodríguez-López, J.; Parks, J. J.; Ritzert, N. L.; Ralph, D. C.; Abruña, H. D. Reactivity of monolayer chemical

vapor deposited graphene imperfections studied using scanning electrochemical microscopy. *ACS Nano* **2012**, *6*, 3070–3079.

[6] Rodríguez-López, J.; Ritzert, N. L.; Mann, J. A.; Tan, C.; Dichtel, W. R.; Abruña, H. D. Quantification of the surface diffusion of tripodal binding motifs on graphene using scanning electrochemical microscopy. *J. Am. Chem. Soc.* **2012**, *134*, 6224–6236.

[7] Roberts, W. S.; Lonsdale, D. J.; Griffiths, J.; Higson, S. P. J. Advances in the application of scanning electrochemical microscopy to bioanalytical systems. *Biosens. Bioelectron.* **2007**, *23*, 301–318.

[8] Parra, A.; Casero, E.; Vázquez, L.; Jin, J.; Pariente, F.; Lorenzo, E. Microscopic and voltammetric characterization of bioanalytical platforms based on lactate oxidase. *Langmuir* **2006**, *22*, 5443–5450.

[9] Horrocks, B. R.; Wittstock, G. Biotechnological applications. In *Scanning Electrochemical Microscopy*; Mirkin, M. V.; Bard, A. J., Eds.; CRC Press: Boca Raton, 2012; pp 318–370.

[10] Edwards, M. A.; Martin, S.; Whitworth, A. L.; Macpherson, J. V.; Unwin, P. R. Scanning electrochemical microscopy: Principles and applications to biophysical systems. *Physiol. Measure.* **2006**, *27*, R63–R108.

[11] Pierce, D. T.; Unwin, P. R.; Bard, A. J. Scanning electrochemical microscopy. 17. Studies of enzyme-mediator kinetics for membrane- and surface-immobilized glucose oxidase. *Anal. Chem.* **1992**, *64*, 1795–1804.

[12] Pellissier, M.; Zigah, D.; Barrière, F.; Hapiot, P. Optimized preparation and scanning electrochemical microscopy analysis in feedback mode of glucose oxidase layers grafted onto conducting carbon surfaces. *Langmuir* **2008**, *24*, 9089–9095.

[13] Nogala, W.; Szot, K.; Burchardt, M.; Roelfs, F.; Rogalski, J.; Opallo, M.; Wittstock, G. Feedback mode SECM study of laccase and bilirubin oxidase immobilised in a sol-gel processed silicate film. *Analyst* **2010**, *135*, 2051–2058.

[14] Zhao, C.; Wittstock, G. Scanning electrochemical microscopy for detection of biosensor and biochip surfaces with immobilized pyrroloquinoline quinone (PQQ)-dependent glucose dehydrogenase as enzyme label. *Biosens. Bioelectron.* **2005**, *20*, 1277–1284.

[15] Schäfer, D.; Maciejewska, M.; Schuhmann, W. SECM visualization of spatial variability of enzyme–polymer spots: 1. Discretisation and interference elimination using artificial neural networks. *Biosens. Bioelectron.* **2007**, *22*, 1887–1895.

[16] Zhao, C.; Wittstock, G. Scanning electrochemical microscopy of quinoprotein glucose dehydrogenase. *Anal. Chem.* **2004**, *76*, 3145–3154.

[17] Wittstock, G.; Schuhmann, W. Formation and imaging of microscopic enzymatically active spots on an alkanethiolate-covered gold electrode by scanning electrochemical microscopy. *Anal. Chem.* **1997**, *69*, 5059–5066.

[18] Zhao, C.; Sinha, J. K.; Wijayawardhana, C. A.; Wittstock, G. Monitoring β-galactosidase activity by means of scanning electrochemical microscopy. *J. Electroanal. Chem.* **2004**, *561*, 83–91.

[19] Arrigan, D. W. M. Nanoelectrodes, nanoelectrode arrays and their applications. *Analyst* **2004**, *129*, 1157–1165.

[20] Katemann, B. B.; Schuhmann, W. Fabrication and characterization of needle-type. *Electroanalysis* **2002**, *14*, 22–28.

[21] Shao, Y. H.; Mirkin, M. V.; Fish, G.; Kokotov, S.; Palanker, D.; Lewis, A. Nanometer-sized electrochemical sensors. *Anal. Chem.* **1997**, *69*, 1627–1634.

[22] Murray, R. W. Nanoelectrochemistry: Metal nanoparticles, nanoelectrodes, and nanopores. *Chem. Rev.* **2008**, *108*, 2688–2720.

[23] Mirkin, M. V.; Fan, F.-R. F.; Bard, A. J. Scanning electrochemical microscopy part 13. Evaluation of the tip shapes of nanometer size microelectrodes. *J. Electroanal. Chem.* **1992**, *328*, 47–62.

[24] Melmed, A. J. The art and science and other aspects of making sharp tips. *J. Vacuum Sci. Technol. B: Microelectron. Nanometer Struct. Process. Measure. Phenom.* **1991**, *9*, 601–608.

[25] Bach, C. E.; Nichols, R. J.; Beckmann, W.; Meyer, H.; Schulte, A.; Besenhard, J. O.; Jannakoudakis, P. D. Effective insulation of scanning tunneling microscopy tips for electrochemical studies using an electropainting method. *J. Electrochem. Soc.* **1993**, *140*, 1281–1284.

[26] Slevin, C. J.; Gray, N. J.; Macpherson, J. V.; Webb, M. A.; Unwin, P. R. Fabrication and characterisation of nanometre-sized platinum electrodes for voltammetric analysis and imaging. *Electrochem. Commun.* **1999**, *1*, 282–288.

[27] Zhang, B.; Galusha, J.; Shiozawa, P. G.; Wang, G. L.; Bergren, A. J.; Jones, R. M.; White, R. J.; Ervin, E. N.; Cauley, C. C.; White, H. S. Bench-top method for fabricating glass-sealed nanodisk electrodes, glass nanopore electrodes, and glass nanopore membranes of controlled size. *Anal. Chem.* **2007**, *79*, 4778–4787.

[28] Macpherson, J. V.; Unwin, P. R. Combined scanning electrochemical–atomic force microscopy. *Anal. Chem.* **2000**, *72*, 276–285.

[29] Li, Y. X.; Bergman, D.; Zhang, B. Preparation and electrochemical response of 1−3 nm Pt disk electrodes. *Anal. Chem.* **2009**, *81*, 5496–5502.

[30] Watkins, J. J.; Chen, J. Y.; White, H. S.; Abruña, H. D.; Maisonhaute, E.; Amatore, C. Zeptomole voltammetric detection and electron-transfer rate measurements using platinum electrodes of nanometer dimensions. *Anal. Chem.* **2003**, *75*, 3962–3971.

[31] Pendley, B. D.; Abruna, H. D. Construction of submicrometer voltammetric electrodes. *Anal. Chem.* **1990**, *62*, 782–784.

[32] Agyekum, I.; Nimley, C.; Yang, C. X.; Sun, P. Combination of scanning electron microscopy in the characterization of a nanometer-sized electrode and current fluctuation observed at a nanometer-sized electrode. *J. Phys. Chem. C* **2010**, *114*, 14970–14974.

[33] Baltes, N.; Thouin, L.; Amatore, C.; Heinze, J. Imaging concentration profiles of redox-active species with nanometric amperometric probes: Effect of natural convection on transport at microdisk electrodes. *Angew. Chem., Int. Ed.* **2004**, *43*, 1431–1435.

[34] Schulte, A.; Chow, R. H. A simple method for insulating carbon-fiber microelectrodes using anodic electrophoretic deposition of paint. *Anal. Chem.* **1996**, *68*, 3054–3058.

[35] Conyers, J. L.; White, H. S. Electrochemical characterization of electrodes with submicrometer dimensions. *Anal. Chem.* **2000**, *72*, 4441–4446.

[36] Watkins, J. J.; White, H. S. The role of the electrical double layer and ion pairing on the electrochemical oxidation of hexachloroiridate(III) at Pt electrodes of nanometer dimensions. *Langmuir* **2004**, *20*, 5474–5483.

[37] Sun, P.; Zhang, Z. Q.; Guo, J. D.; Shao, Y. H. Fabrication of nanometer-sized electrodes and tips for scanning electrochemical microscopy. *Anal. Chem.* **2001**, *73*, 5346–5351.

[38] Liu, B.; Rolland, J. P.; DeSimone, J. M.; Bard, A. J. Fabrication of ultramicroelectrodes using a “Teflon-like” coating material. *Anal. Chem.* **2005**, *77*, 3013–3017.

[39] Fan, F.-R. F.; Bard, A. J. Electrochemical detection of single molecules. *Science* **1995**, *267*, 871–874.

[40] Fan, F.-R. F.; Kwak, J.; Bard, A. J. Single molecule electrochemistry. *J. Am. Chem. Soc.* **1996**, *118*, 9669–9675.

[41] Bard, A. J.; Fan, F.-R. F. Electrochemical detection of single molecules. *Acc. Chem. Res.* **1996**, *29*, 572–578.

[42] Penner, R. M.; Heben, M. J.; Longin, T. L.; Lewis, N. S. Fabrication and use of nanometer-sized electrodes in electrochemistry. *Science* **1990**, *250*, 1118–1121.

[43] Hrapovic, S.; Luong, J. H. T. Picoamperometric detection of glucose at ultrasmall platinum-based biosensors: Preparation and characterization. *Anal. Chem.* **2003**, *75*, 3308–3315.

[44] Tel-Vered, R.; Bard, A. J. Generation and detection of single metal nanoparticles using scanning electrochemical microscopy techniques. *J. Phys. Chem. B* **2006**, *110*, 25279–25287.

[45] Lai, S. C. S.; Dudin, P. V.; Macpherson, J. V.; Unwin, P. R. Visualizing zeptomole (electro)catalysis at single nanoparticles within an ensemble. *J. Am. Chem. Soc.* **2011**, *133*, 10744–10747.

[46] Kim, J.; Renault, C.; Nioradze, N.; Arroyo-Currás, N.; Leonard, K. C.; Bard, A. J. Electrocatalytic activity of individual Pt nanoparticles studied by nanoscale scanning electrochemical microscopy. *J. Am. Chem. Soc.* **2016**, *138*, 8560–8568.

[47] Abad, J. M.; Tesio, A. Y.; Pariente, F.; Lorenzo, E. Patterning gold nanoparticle using scanning electrochemical microscopy. *J. Phys. Chem. C* **2013**, *117*, 22087–22093

[48] Ferreira, M.; Varela, H.; Torresi, R. M.; Tremiliosi-Filho, G. Electrode passivation caused by polymerization of different phenolic compounds. *Electrochim. Acta* **2006**, *52*, 434–442.

[49] Llopis, J. F.; Colom; F. Encyclopedia of electrochemistry of the elements. In *Encyclopedia of Electrochemistry of the Elements*; Bard, A. J., Ed.; Marcel Dekker: New York, 1976; Vol. 6, pp 224–226.

[50] Haiss, W.; Martín, S.; Leary, E.; van Zalinge, H.; Higgins, S. J.; Bouffier, L.; Nichols, R. J. Impact of junction formation method and surface roughness on single molecule conductance. *J. Phys. Chem. C* **2009**, *113*, 5823–5833.

[51] Brust, M.; Bethell, D.; Kiely, C. J.; Schiffrin, D. J. Self-assembled gold nanoparticle thin films with nonmetallic optical and electronic properties. *Langmuir* **1998**, *14*, 5425–5429.

[52] Love, J. C.; Estroff, L. A.; Kriebel, J. K.; Nuzzo, R. G.; Whitesides, G. M. Self-assembled monolayers of thiolates on metals as a form of nanotechnology. *Chem. Rev.* **2005**, *105*, 1103–1170.

[53] Aizenberg, J.; Black, A. J.; Whitesides, G. M. Controlling local disorder in self-assembled monolayers by patterning the topography of their metallic supports. *Nature* **1998**, *394*, 868–871.

[54] Madoz-Gúrpide, J.; Abad, J. M.; Fernández-Recio, J.; Vélez, M.; Vázquez, L.; Gómez-Moreno, C.; Fernández, V. M. Modulation of electroenzymatic NADPH oxidation through oriented immobilization of ferredoxin:$NADP^+$ reductase onto modified gold electrodes. *J. Am. Chem. Soc.* **2000**, *122*, 9808–9817.

[55] Darder, M.; Takada, K.; Pariente, F.; Lorenzo, E.; Abruña, H. D. Dithiobissuccinimidyl propionate as an anchor for assembling peroxidases at electrodes surfaces and its application in a H_2O_2 biosensor. *Anal. Chem.* **1999**, *71*, 5530–5537.

[56] Leiros, I.; Wang, E.; Rasmussen, T.; Oksanen, E.; Repo, H.; Petersen, S. B.; Heikinheimo, P.; Hough, E. The 2.1 Å structure of *Aerococcus viridans* l-lactate oxidase (LOX). *Acta Cryst.* **2006**, *62*, 1185–1190.

[57] Parra, A.; Casero, E.; Vázquez, L.; Pariente, F.; Lorenzo, E. Design and characterization of a lactate biosensor based on immobilized lactate oxidase onto gold surfaces. *Anal. Chim. Acta* **2006**, *555*, 308–315.